J Clust Sci (2011) 22:473–489
DOI 10.1007/s10876-011-0395-1

ORIGINAL PAPER

Theoretical Study of Hydrogen Adsorption on Ruthenium Clusters

Gui-Xian Ge · Hong-Xia Yan · Qun Jing · You-Hua Luo

Received: 4 May 2011 / Published online: 22 June 2011
© The Author(s) 2011. This article is published with open access at Springerlink.com

Abstract The geometries, stabilities, electronic, and magnetic properties of hydrogen adsorption on Ru_n clusters have been systematically investigated by using density functional theory with generalized gradient approximation. The result indicates the absorbed species does not lead to a rearrangement of the basic cluster. For $n > 2$, three different adsorption patterns are found for the Ru_nH_2 complexes: One H atom binds to the Ru top site, and another H binds to the bridge site for $n = 3, 5, 6, 8$; bridge site adsorption for $n = 4$; hollow site and top site adsorption for $n = 7$. The adsorption energies display oscillation and reach the peak at $n = 2$, 4, 7, implying their high chemical reactivity. The small electron transferred number between H atoms and Ru_n clusters indicates that the interaction between H atoms and Ru_n clusters is small. When H_2 is absorbed on the Ru_n clusters, the chemical activity of corresponding clusters is dramatically increased. The absorbed H_2 can lead to an oscillatory behavior of the magnetic moments, and this behavior is rooted in the electronic structure of the preceding cluster and the changes in the magnetic moment are indicative of the relative ordering of the majority and minority LUMO's. The second order difference indicates 5 is magic number in Ru_nH_2 and Ru_n clusters.

Keywords Ru_nH_2 cluster · Electronic properties · Equilibrium geometries

G.-X. Ge (✉) · H.-X. Yan · Q. Jing
Key Laboratory of Ecophysics and Department of Physics, School of Sciences, Shihezi University, Xinjiang 832003, China
e-mail: geguixian@126.com

Y.-H. Luo
Department of Physics, East China University of Science and Technology, Shanghai 200237, China

Y.-H. Luo
Institute for Theoretical Physics, Henan University, Kaifeng 475001, China

Introduction

In the past 20 years, small metal clusters have been used to model the adsorption of different molecules with the purpose to obtain a good description of the activity of many metal catalysts. Due to the small particles size of a well dispersed catalysts, most or almost all of its atom are surface atoms, so they exhibit structural and reaction properties different from those of the bulk, they are appropriate to surface reactions as the most process in catalysis are. Many previous researches showed that the catalytic properties of clusters are structure dependent, leading to different adsorption energies and sites for different structures of clusters [1–6]. Hydrogen is employed in many modern technologies [7–21], so surface reactions of hydrogen molecules in transition metals have been carried out over the adsorption and desorption of hydrogen and deuterium molecules on well-defined single crystal metals. Axel Pramann et al. [22] studied hydrogen chemisorption rates and electronic structures of small Nb_nAl^- clusters by photoelectron spectroscopic method. Poulain et al. [23] studied the C_{2v} and C_{3v} reaction of H_2 with a Pt_4 cluster. Hege Strmsnes et al. [24] studied the chemisorption of molecular hydrogen on a seven atom gold cluster using explicitly correlated wave functions. On the other hand, an area that has attracted recent attention is the effect of chemisorption on the magnetic properties of clusters. For example, Whetten et al. [25] studied the reactivity of Fe_n clusters toward H_2 and D_2, and found the Fermi energy and the band filling could be modulated by adding hydrogen suggests that one could expect interesting effects on magnetic properties. Indeed, Knickelbein et al. [26] recently investigated the effect of hydrogen on the magnetic moment of Fe_n clusters in molecular beam experiments and found intriguing results. Knickelbein et al. generated Fe_n clusters containing 10–25 atoms in molecular beams and the clusters were saturated with hydrogen. The hydrogenated clusters were subsequently passed through the Stern Gerlach gradient fields. They found that unlike the case of larger nanoparticles and thin films where the hydrogen adsorption quenches the magnetic moment [27], the magnetic moments of the saturated hydrogenated clusters containing 12–25 atoms were higher than those of the free clusters.

Ruthenium is the main element used for hydrogenation and dehydrogenation catalytic reactions. Liu et al. [28] studied adsorption characteristics of atomic nitrogen on ruthenium surfaces, they found that atomic nitrogen always preferably occupies the high coordination sites on Ru surfaces. Carmelo Crisafulli et al. [29] have studied Ni-Ru bimetallic catalysts for the CO_2 reforming of methane. Romain Berthoud et al. [30] have studied hydrogen and oxygen adsorption stoichiometries on silica supported ruthenium nanoparticles. Zheng et al. [31] have investigated NH_3 decomposition kinetics on supported Ru clusters. Tu et al. [32] have studied the interaction of oxygen with ruthenium clusters by density functional study. Suss-Fink et al. [33] investigated the cluster dication $[H_6Ru_4(C_6H_6)_4]^{2+}$ using the a low-temperature ^{1}H-NMR and density functional theory (DFT) calculations, and found the cluster dication $[H_6Ru_4(C_6H_6)_4]^{2+}$(1) tends to loose molecular hydrogen to form the cluster dication $[H_4Ru_4(C_6H_6)_4]^{2+}$(2). The equilibrium between **1** and **2** can be used for catalytic hydrogenation reactions. Adams et al. investigated the Activation of hydrogen by mixed transitional metal cluster complex [34–37]. Poteau et al. [38]

studied spectroscopic and thermodynamic properties of surfacic hydrides on Ru (0001) model surface: the influence of the coordination modes and the coverage by density functional theory and this study partially opens the route to DFT studies of multistep hydrogenation reactions at the surface of ruthenium nanoparticles monitored by spectroscopic techniques. Torsten Gutmann et al. [39] studied hydrido-ruthenium cluster complexes as models for reactive surface hydrogen species of ruthenium nanoparticles by solid-state ^{2}H NMR and quantum chemical calculations and found that the ^{2}H nuclear quadrupolar interaction is a sensitive tool for distinguishing the binding state of the deuterons to the transition metal.

To our knowledge, the study on the adsorption properties of small molecule on ruthenium clusters is still lacking either experimentally or theoretically so far. It would be interesting to know the adsorption ability of ruthenium clusters to small molecules such as the H_2 molecule. More precisely, where are the optimal adsorption sites of ruthenium clusters to H_2 molecule? Moreover, how does the adsorption of H_2 molecule affect the magnetism of the clusters? To answer these questions, we have performed density functional theory (DFT) computations to explore the adsorption behavior of H_2 molecule on Ru_n clusters. The purposes of this paper include the following: (a) Locate the optimal adsorption sites and (b) analyze the size-dependent structural, electronic, and magnetic properties of the Ru_nH_2 complexes, and compare with the bare ruthenium clusters.

Computational Methods

Full geometry optimizations were performed using the spin-polarized density functional theory (DFT) implemented in a DMOL package [40]. In the electronic structure calculations, all electron treatment and double numerical basis including *d*-polarization function (DNP) [40] were chosen. The exchange–correlation interaction was treated within the generalized gradient approximation (GGA) using PBE functional. Self-consistent field calculations were done with a convergence criterion of 10^{-5} Hartree on the total energy. The density mixing criterion for charge and spin were 0.2 and 0.5, respectively. The Direct Inversion in an Iterative Subspace (DIIS) approach was used to speed up SCF convergence. A 0.001 Hartree of smearing was applied to the orbital occupation. In the geometry optimization, the converged thresholds were set to 0.004 Hartree/Å for the forces, 0.005Å for the displacement and 10^{-5} Hartree for the energy change. Harmonic vibrational frequencies were calculated for the promising stationary points from a direct structural optimization; if an imaginary vibrational mode was found, a relaxation along coordinates of imaginary vibrational mode was carried out until the true local minimum was actually obtained. Therefore, all isomers for each cluster are guaranteed as the local minima. The on-site charges and magnetic moment were evaluated via Mulliken population analysis [41].

To test the accuracy of the theoretical method, we have calculated the dimers for Ru_2 and H_2 by using different functionals. For Ru_2, the bond length $r = 2.26$ Å, $\omega = 364.46$ cm^{-1}; the calculated results using PBE functional are in agreement with the previous theory values obtained by all-electron calculation ($r = 2.41$Å,

$\omega = 380\ cm^{-1}$) [42] and experimental value by Resonance Raman matrix isolation studies of mass-selected (347.1(9) cm^{-1}) [43]. For H_2, the bond length $r = 0.748$Å, binding energy $E_b = 4.665$ eV, $\omega = 4410.896\ cm^{-1}$. The calculated results using PBE functional are in good agreement with experiment values ($r = 0.741$Å, $E_b = 4.519$ eV $\omega = 4401.21\ cm^{-1}$) [44]. It indicates that the employed PBE scheme is reliable for the dimer Ru_2 and H_2. Consequently, the PBE functional are reliable and accurate enough to be applied to describe the properties of the Ru_nH_2 in this paper.

Results and Discussions

Equilibrium Structures

The low-lying isomers of Ru_nH_2 complexes and their naked counterparts Ru_n are displayed in Figs. 1 and 2. The structure and the bond length of the lowest energy structures for Ru_n and Ru_nH_2 are given in Table 1. Here we only present the longest and the shortest interatomic distances between two Ru atoms, two H atoms and Ru–H in Ru_nH_2 and in the corresponding bare Ru_n. The geometries of Ru_nH_2 and Ru_n clusters with considered spin configuration are performed by DFT. The lowest energy geometry of Ru_2 is a linear structure. For Ru_3, the result is different from those of empirical methods by Tu et al. [45] who have all concluded that the structure of Ru_3 is an equilateral triangle. The lowest energy structure we obtained is a triangle (C_s) whose binding energy is 0.819 eV lower than that of equilateral structure. The lowest energy geometry of Ru_4 is a quadrangle structure with D_{4h} symmetry. The distorted tetrahedron is 0.348 eV higher than that of the lowest energy geometry. For Ru_5, the lowest energy structure is a square pyramid. The trigonal bi-pyramid is an isomer with 0.853 eV higher than the square pyramid. A trigonal prism is the lowest energy structure of Ru_6 cluster. The square bipyramid is 0.358 eV higher than that of trigonal prism. The lowest energy structure of Ru_7 is a twin square pyramid. The trigonal prism structure face capped a Ru atom is a matastable isomer, it's energy is 0.0269 eV higher than that of the twin square pyramid. A square prism is the lowest energy structure of Ru_8 cluster. Most of lowest energy structures we obtained are similar to the result obtained by Tu et al. [45].

For RuH_2, the ground state corresponds to a H–H distance of 2.428Å. The H molecular is therefore activated. For Ru_2, the additional hydrogen molecular occupies the on-top site. The Ru–Ru bond length (R_{Ru-Ru}) is 2.322Å, 4.31% greater than that in the bare Ru_2 dimer. The two Ru–H bond lengths are 1.573 and 1.574Å, respectively. Two Ru–Ru–H angles are both around 90 degree. The H–H bond length (R_{H-H}) is 2.173Å, again indicates that the H_2 is activated compared with free H_2 molecular.

For $n > 2$, three different adsorption patterns are found for the Ru_nH_2 complexes: one H is absorbed on the Ru top site, and another H is absorbed on the bridge site which H atom sits over the Ru–Ru bond for $n = 3, 5, 6, 8$; bridge site adsorption for $n = 4$; hollow site and top site adsorption for $n = 7$. The longest R_{Ru-Ru} bond

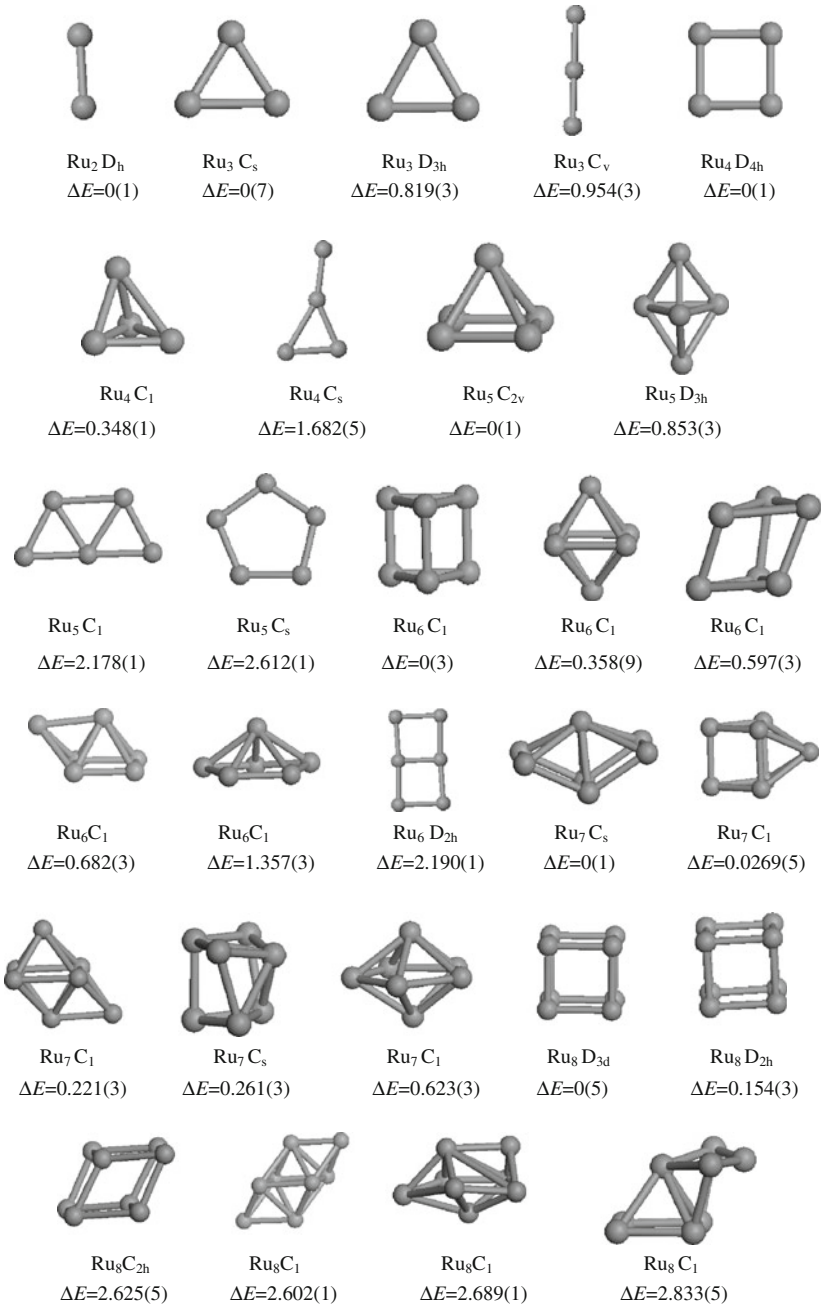

Fig. 1 Ground state and some matastable geometries of Ru_n clusters. ΔE(eV) is the excess energy of an isomer as compared to the energy of the most stable one. The multiplicity is given in *parentheses*

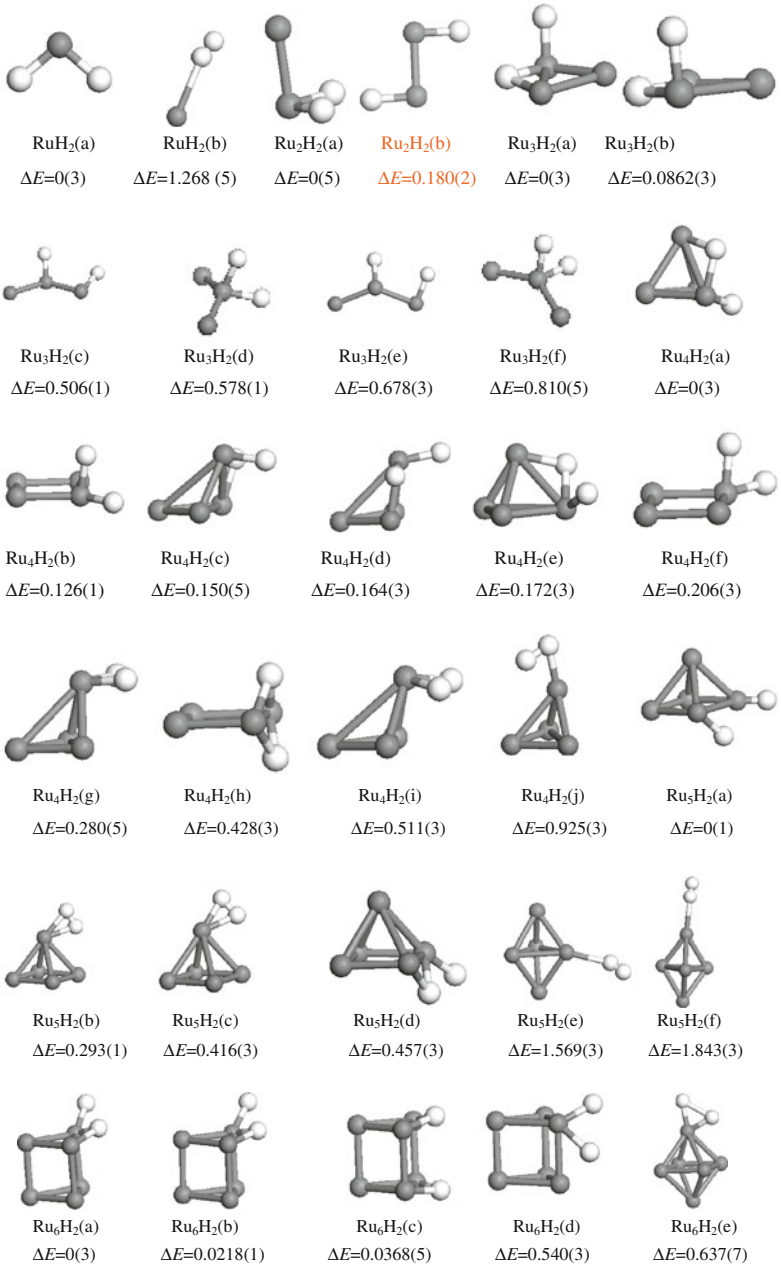

Fig. 2 Ground state and some matastable geometries of Ru_nH_2 clusters. The *dark circles* are the Ru atoms while the *white circles* are the H atoms. ΔE(eV) is the excess energy of an isomer as compared to the energy of the most stable one. The multiplicity is given in *parentheses*. The symmetry groups of Ru_nH_2 clusters are C_1 except that of the most stable Ru_nH_2(n = 1, 4) (C_s, C_{2v})

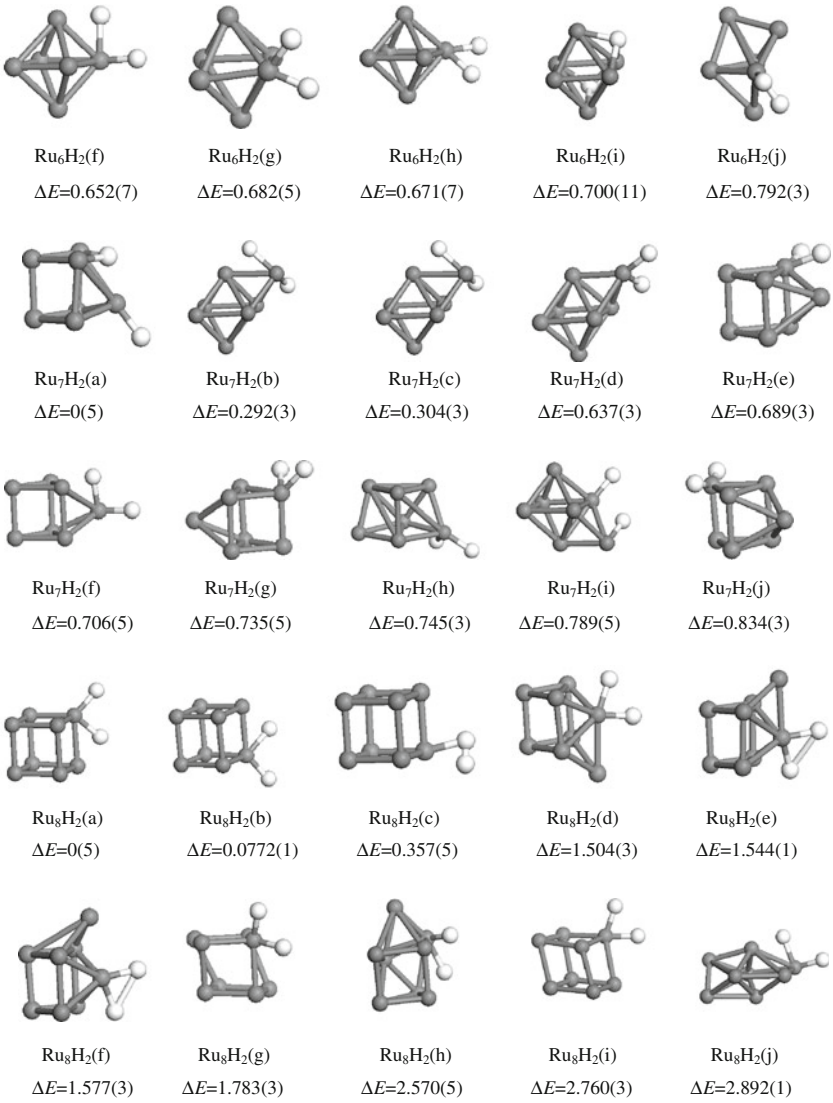

Fig. 2 continued

lengths range from 2.493 to 2.598 Å and the shortest from 2.326 to 2.399 Å, the longest $R_{Ru–H}$ bond lengths vary from 1.743 to 1.849 Å and the shortest from 1.154 to 1.722 Å, and the bond lengths of H–H are in the range of 2.320 to 3.419 Å, which indicates the H_2 is activated.

For Ru_2H_2, the ground state is quintet state with H–H bond length of 2.173 Å. When one H atom is drawn to one Ru atom and the other H atom to the other Ru atom, the optimized structure (Fig. 2b) is 0.18 eV higher than the ground state. In this structure, both of Ru–Ru–H angles are about 90°.

Table 1 The longest (Max_R_{Ru-Ru}, Max_R_{Ru-H}) and the shortest (Min_R_{Ru-Ru}, Min_R_{Ru-H}) bond lengths(Å) and H–H bond length(Å)(R_{H-H}) of the lowest energy structures of Ru_n clusters and Ru_nH_2 complexes

n	Symmetry		Max_R_{Ru-Ru}		Min_ R_{Ru-Ru}		Max_R_{Ru-H}	Min_ R_{Ru-H}	R_{H-H}
	Ru_nH_2	Ru_n	Ru_nH_2	Ru_n	Ru_nH_2	Ru_n	Ru_nH_2	Ru_nH_2	Ru_nH_2
2	C_1	$D_{\infty h}$	2.322	2.226	2.322	2.226	1.574	1.573	2.173
3	C_1	C_s	2.598	2.505	2.326	2.343	1.748	1.581	2.443
4	C_s	D_{4h}	2.587	2.303	2.399	2.303	1.780	1.722	2.530
5	C_1	C_{2v}	2.584	2.536	2.313	2.341	1.787	1.154	2.407
6	C_1	C_1	2.542	2.459	2.325	2.342	1.795	1.661	2.571
7a	C_1	C_s	2.898	2.637	2.343	2.339	1.849	1.632	3.419
7b	C_1	C_1	2.610	2.609	2.398	2.338	1.810	1.750	2.988
8	C_1	D_{3d}	2.493	2.370	2.336	2.363	1.743	1.633	2.320

The most stable structure of Ru_3H_2 is a triplet state with C_1 symmetry. The structure with a H is absorbed on the different top site is metastable isomer, its energy is 0.0861 eV higher than that of the lowest energy structure. In case of Ru_4H_2, the first and the second H are both absorbed on the adjacent bridge sites. In the lowest energy structure with a triplet state, the H–H distance is 2.530 Å, and the H_2 is also activated. The structure with two H atoms absorbed on the top site on the lowest energy structure of Ru_4 is metastable isomer, its energy is 0.126 eV higher than that of the lowest energy structure. For Ru_5H_2, a square pyramid-based structure in a singlet state is most stable, followed by a singlet, triplet and triplet state with 0.293, 0.416 and 0.457 eV higher in energy, respectively.

In the case of Ru_6H_2, the most stable structure is a trigonal prism-based structure in a triplet state, followed by a singlet with 0.0218 eV higher in energy than the most stable structure. The structure with two H atoms absorbed on the bridge site on the trigonal prism is metastable isomer, the energy is 0.0368 eV higher than that of the lowest energy structure. For Ru_7H_2, the most stable structure is a singly capped trigonal prism-based structure in a quintuple state, formed by a hollow site adsorption in which one H atom sits above the plane of three Ru atoms and another H atom locates on the Ru atom top. The secondary low-lying isomer of Ru_7H_2 is a singly capped square bi-pyramid-based structure, which actually corresponds to the third low-lying isomer of pure Ru_7 isomer. Other isomers are also presented in Fig. 2. The lowest energy structure of Ru_8H_2 is square prism-based structure in a quintet state, the single state is 0.0772 eV higher in energy.

According to above analysis, it is shown that the lowest energy structure of Ru_nH_2 can be obtained by adsorbing H_2 in the lowest energy and some meta-table isomers of Ru_n clusters. It is interesting to notice that in all cases, the absorbed species does not lead to a rearrangement of the basic cluster, but the hydrogen atom adsorbs to the edge of a Ru–Ru bond with the bond lengthening. The longest and the shortest R_{Ru-Ru} (increase with the cluster size overall) as well as R_{Ru-H} vary in small ranges overall. In the Ru_nH_2, H–H bond length is about 2.173–3.419 Å. The values

are larger than the bond length of optimized H_2 (0.748 Å), which indicates the hydrogen molecular is activated.

Relatives Stability and Electronic Properties

It is known that the relative stability of the different sized cluster can be predicted by calculating the averaged binding energy. The averaged binding energy can be defined as the following formula:

$$E_b[\mathrm{Ru}_n\mathrm{H}_2] = (-E[\mathrm{Ru}_n\mathrm{H}_2] + nE[\mathrm{Ru}] + 2E[\mathrm{H}])/(n+2) \quad (1)$$

$$E_b[\mathrm{Ru}_n] = (-E[\mathrm{Ru}_n] + nE[\mathrm{Ru}])/n \quad (2)$$

where E_T ($\mathrm{Ru}_n\mathrm{H}_2$), E_T (Ru),E_T (H) and E_T (Ru_n) represent the total energies of the $\mathrm{Ru}_n\mathrm{H}_2$, Ru, H, Ru_n clusters, respectively. The calculated results on the averaged energies for $\mathrm{Ru}_n\mathrm{H}_2$ and Ru_n clusters are plotted in Fig. 3. When H_2 is adsorbed on the Ru_n clusters, the average binding energy is larger than that of Ru_n clusters for $n = 2$–3, the average binding energy is smaller than that of Ru_n clusters with cluster size increasing. For $n = 2$–3, the H atom mainly act with Ru atom. The calculated binding energy (3.577 eV) of Ru–H are larger than that of Ru–Ru (3.19 eV), which indicates the interaction between Ru and H is larger than that of Ru–Ru. So the averaged energy for $\mathrm{Ru}_n\mathrm{H}_2$ clusters is larger than that of Ru_n. When $n > 3$, the H atoms are mainly bond Ru_n by the weak interaction, which causes the averaged binding energies of $\mathrm{Ru}_n\mathrm{H}_2$ are smaller than that of Ru_n clusters.

The relative stabilities of these clusters can be better understood by calculating the incremental formation energies, i.e., the second order difference of cluster energies, we defined the $\Delta_2 E(n)$ as the following formula:

$$\Delta_2 E = E(n-1) + E(n+1) - 2E(n) \quad (3)$$

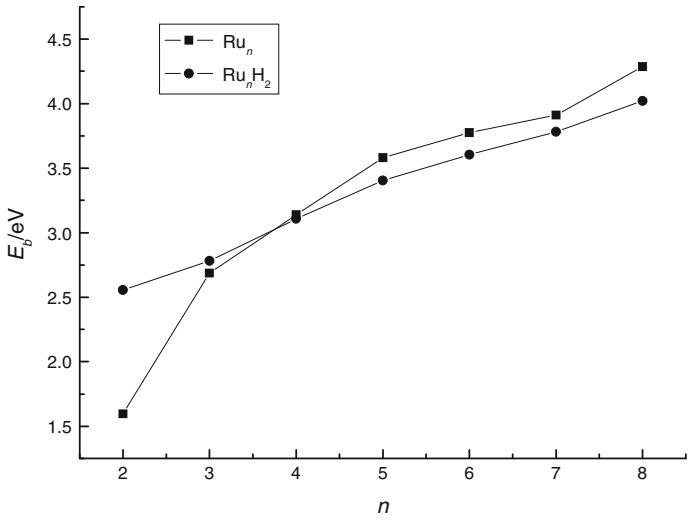

Fig. 3 Binding energy versus cluster size for $\mathrm{Ru}_n\mathrm{H}_2$ and Ru_n clusters

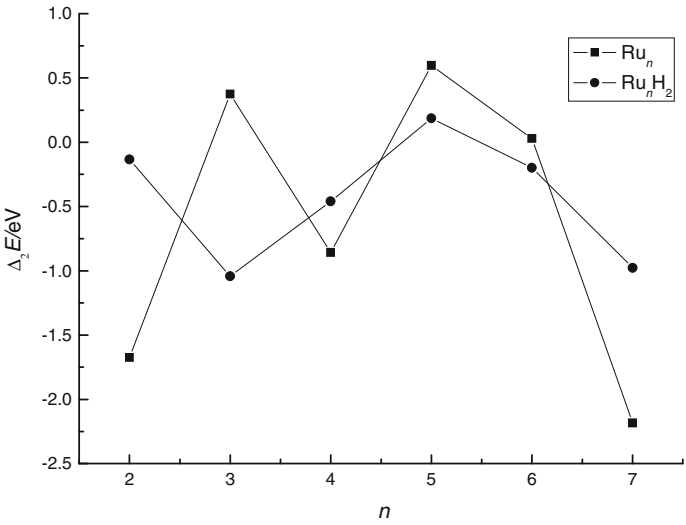

Fig. 4 Second finite difference of the total energies for Ru_nH_2 and Ru_n clusters

where E_T (n) is the total energy of clusters. The second order difference of cluster energies for Ru_nH_2 and Ru_n clusters are all presented in Fig. 4. According to Fig. 4, for Ru_n clusters, the peak values appear at $n = 3$, 5, it shows apparently that the maximum magic number of the relative stability is $n = 3$, 5 among investigated Ru_n clusters. For Ru_nH_2, particularly high peaks for are found at $n = 5$, reflecting that the Ru_5H_2 cluster is more stable than its neighboring clusters. The same magic number 5 indicates the effect of H molecular to the bonding natures of Ru_n clusters is small for $n > 3$, which is consistent with the result of the averaged energy.

To measure the strength of the interaction of H with each of the clusters, we calculated the binding energy of H to each cluster according to:

$$E(H) = E(\mathrm{Ru}_n\mathrm{H}_2) - E(\mathrm{Ru}_n) - 2E(\mathrm{H}) \tag{4}$$

The calculated binding energies of H to cluster corresponding to the most energetically favorable chemisorption site are show in Fig. 5, which has a strong dependence on the clusters and increase until $n = 2$, and then decrease to the lowest value of 5.847 eV at $n = 3$. The bind energies of H to Ru_n cluster then increase in general as the size of the clusters increase, attaining the local maxima for $n = 2$, 4 and 7. The larger binding energies of H to Ru_n cluster ($n = 2$, 3) indicate the stronger inaction of Ru–H, which is consistent with the result of the averaged energy. The values for bind energies of H to Ru_n cluster are 5.847–7.024 eV, and these is larger than that of Ru_n cluster(1.597–4.295 eV), which also shows the interaction of Ru–H is larger than that of Ru–Ru.

The electronic properties of clusters are discussed by examining the energy gap between the HOMO and LUMO. The HOMO-LUMO gaps for Ru_nH_2 and Ru_n clusters of the most stable structure are shown in Fig. 6. As can be seen from Fig. 6, when H_2 is absorbed on the Ru_n clusters, the gaps are usually smaller than those of

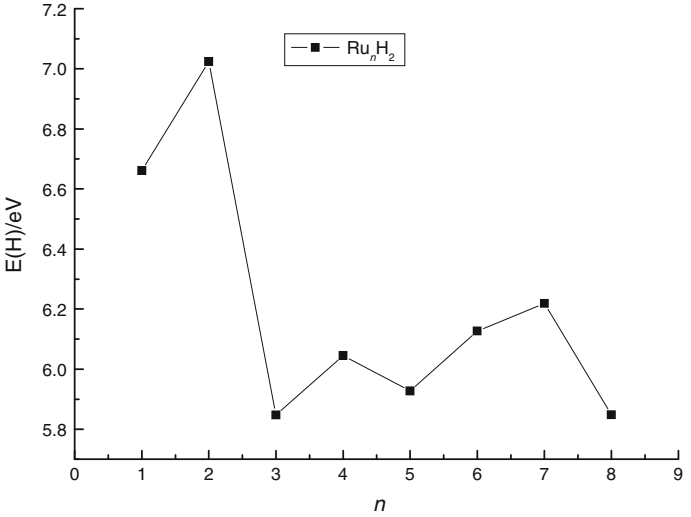

Fig. 5 The binding energies of H to Ru_n clusters

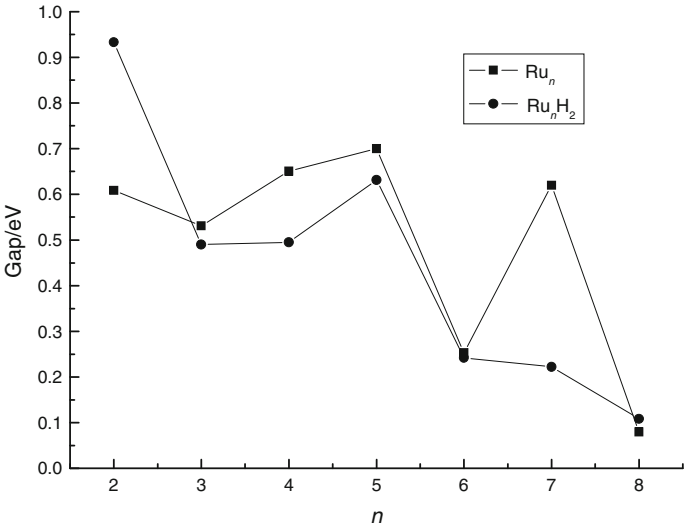

Fig. 6 The HOMO-LUMO Gaps for Ru_nH_2 and Ru_n clusters

Ru_n cluster, which indicates that the adsorption of the H atoms improves the chemical activity of the host clusters in most cases. However, the exceptional case is $n = 2$ in which the values of the gap for Ru_2 are much larger than those of the Ru_2H_2 cluster. Interestingly, the energy gap of Ru_8H_2 is close to that of Ru_8, which shows that the adsorption has little effect on the chemical activity with $n = 8$. Consequently, the Ru_nH_2 clusters exhibit remarkable difference in terms of the variation of the energy gap as the H atoms are adsorbed onto the Ru_n clusters.

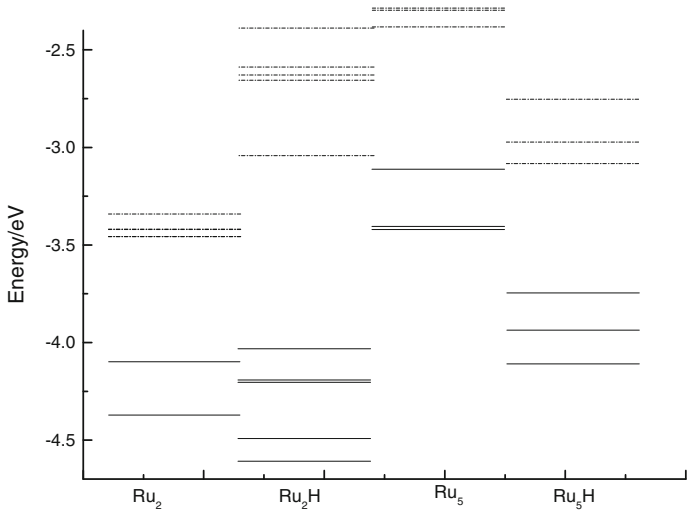

Fig. 7 One electron energy levels in the vicinity of the HOMO and LUMO of the Ru_2H_2, Ru_2, Ru_5H_2, Ru_5 (The *dotted lines* represent the LUMO levels, and the *solid lines* represent HOMO levels)

In light of the particular phenomenon mentioned above, it is necessary to further study the reason about the changing trend of the gap. Meanwhile, the energy level of the molecular orbital for Ru_2 (Ru_2H_2), Ru_5(Ru_5H_2), which is displayed in Fig. 7, were investigated to further illustrate the electronic property. The obvious characteristic of the molecular orbital for Ru_2 is the appearance of the degeneracy of the energy level in the vicinity of the HOMO–LUMO. With the H atoms being adsorbed onto the Ru_2 cluster, the degenerate energy level is completely disappeared. Moreover, compared with Ru_2, the energy level of the LUMO for Ru_2H_2 is elevated strongly (about 0.938 eV). In case of Ru_5, there is also degenerate orbital in the vicinity of HOMO–LUMO. However, the HOMO and LUMO for Ru_5H_2 both consist of two degenerate orbitals, respectively. When H atoms are adsorbed onto the Ru_5 cluster, the LUMO of Ru_5H_2 is also reduced (about 0.669 eV) in comparison to Ru_5. Apparently, the similar behavior of the reduction of the LUMO for $n = 3$, 4, 6, 7, results in the decrease of their energy gap.

In Fig. 8, we give the adsorption energy for Ru_nH_2 complex. The absorbed energy can be defined as the following formula:

$$E_{\text{adv}} = E_{\text{H}_2} + E_{\text{cluster}} - E_{\text{cluster+H}_2} \tag{5}$$

It is well-known that the chemisorption energies can be used to quantitatively describe the reactivity of H_2 on the Ru_n clusters. The calculated chemisorption energies corresponding to the most energetically favorable chemisorption site are show in Fig. 8, which has a strong dependence on the clusters and increase until $n = 2$, and then decrease to the lowest value of 1.182 eV at $n = 3$. The chemisorption energy then increase in general as the size of the clusters increase, attaining the local maxima for $n = 2$, 4 and 7. The present results show the Ru_3 cluster is of high inertness with respect to the H_2 chemisorption, while Ru_2, Ru_4, and Ru_7 clusters are of high activity with respect to the H_2 chemisorption. Note that

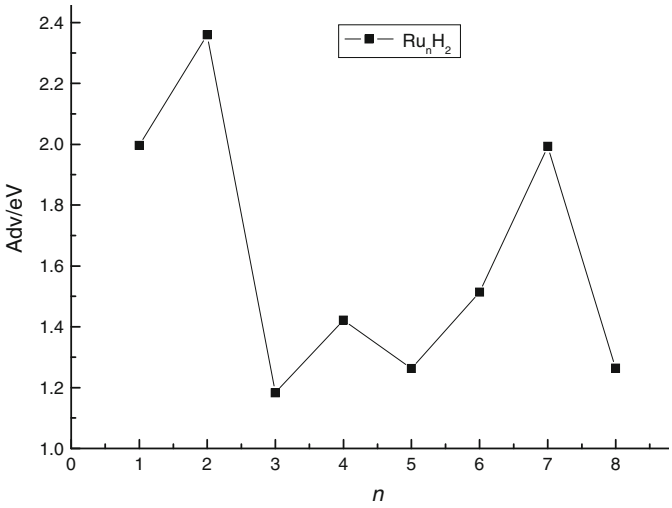

Fig. 8 The absorbed energy (A_{dv}) for Ru_nH_2

Dhilip Kumar et al. [46] also calculated that the H_2 chemisorption energy was found to be the lowest for the stable Ti_7 cluster but highest for the most stable cluster Ti_{13}. Experimental measurements indicate that when Ti_{13} cluster is added as a catalyst to increase the reaction rate of hydrogenation and de hydrogenation processes in alanates [47]. Whether the Ru_2 is added as a catalyst to increase the reaction rate of hydrogenation and de hydrogenation processes is to be studied further theoretically and experimentally.

The charge transfer from the Ru_n cluster to H_2 molecule is an essential factor to determine the H_2 adsorption behavior on Ru_n clusters. Here we give the charge populations from natural population analysis on H atoms (In Fig. 9). According to the NPA charge population, electron transfer will occur from H atoms to Ru_n clusters. The electron transferred number between H atoms and Ru_n clusters is about 0.0475–0.158e, this means the interaction between H atoms and Ru_n clusters is small. When $n = 2, 7$, the charges from H atoms to Ru_n clusters are more, which is consist with the large absorbed energy in these clusters. For Ru_6H_2, the charges from H atoms to Ru_n clusters are smallest among Ru_nH_2 complex, this indicates the adsorption has little effect on Ru_6, which is the reason that the energy gap of Ru_6H_2 is close to that of Ru_6.

Magnetic Properties

Figure 10 gives the spin magnetic moment of pure and hydrogenated clusters. For Ru_3, the H atoms decrease the spin magnetic moment. For Ru_2, Ru_4 and Ru_7, the H atoms increase the spin magnetic moment. In case of Ru_n ($n = 5, 6, 8$), the H atoms have little impact on the spin magnetic moment. In a previous paper, Fournier et al. have proposed H_2 affect on spin magnetic moment of transitional metal clusters can be understood within a simple model [48, 49]. The change in moment is related to

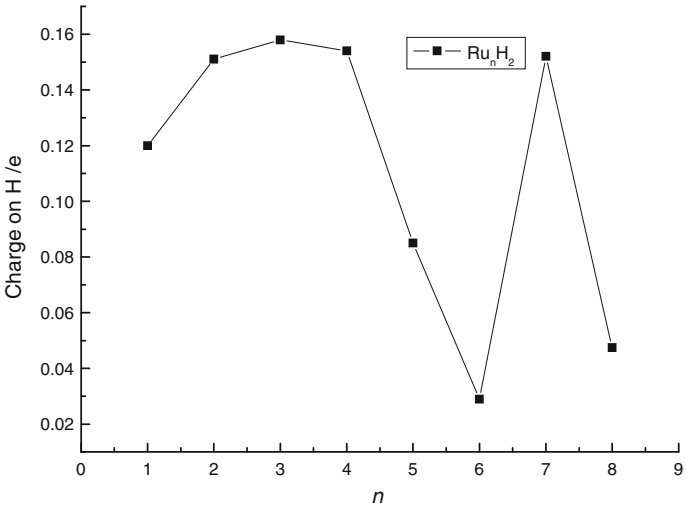

Fig. 9 The averaged charge on the H atoms for Ru_nH_2

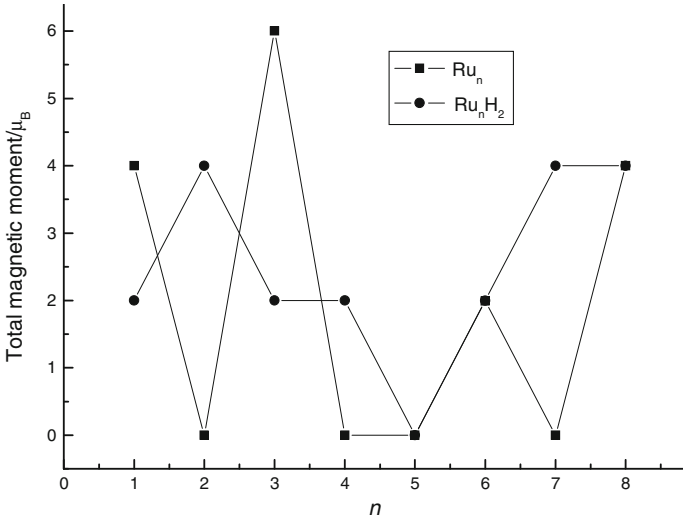

Fig. 10 The total magnetic moment for Ru_nH_2 and Ru_n clusters

the location of the lowest unoccupied orbital of the preceding cluster. The H atom can be considered as a proton and an electron. The additional electron goes to the spin state with lowest LUMO while the proton is screened by the *d*-states of the neighboring Ru sites. This however, is not the only consideration. If the LUMO of the preceding cluster belongs to the minority manifold (spin down) and the LUMO of majority (spin up) is only slightly higher, the additional electron may still go to majority manifold since the exchange coupling could lead to a rearrangement of the manifolds. To put it simply, it is the difference, δE, between the LUMO of the

Table 2 The HOMO and LUMO levels (hartrees) of the majority and minority spin states and δE (eV) in Ru_n and Ru_n H_2 clusters

Cluster	Majority		Minority		
	HOMO	LUMO	HOMO	LUMO	δE
Ru	−0.165049	0.028365	−1.68319	−0.127363	−4.235
RuH_2	−0.192468	−0.085494	−0.175048	−0.126172	−1.105
Ru_2	−0.152441	−0.130001	−0.152425	−0.130039	−0.00103
Ru_2H_2	−0.155393	−0.099403	−0.149725	−0.115411	−0.523
Ru_3	−0.139542	−0.096201	−0.119653	−0.100129	−0.107
Ru_3H_2	−0.145644	−0.127625	−0.145781	−0.118462	0.249
Ru_4	−0.131310	−0.107383	−0.13110	−0.107383	0.000
Ru_4H_2	−0.130210	−0.091910	−0.121221	−0.103016	−0.302
Ru_5	−0.117938	−0.092193	−0.117938	−0.092193	0.000
Ru_5H_2	−0.140009	−0.116785	−0.14009	−0.116785	0.000
Ru_6	−0.112439	−0.103139	−0.116246	−0.102145	0.0270
Ru_6H_2	−0.130284	−0.121382	−0.135251	−0.119575	0.0492
Ru_7	−0.138811	−0.115984	−0.138843	−0.116027	−0.00117
Ru_7H_2	−0.138365	−0.125574	−0.137621	−0.126381	−0.0220
Ru_8	−0.127748	−0.124811	−0.147696	−0.108937	0.432
Ru_8H_2	−0.139109	−0.135132	−0.158438	−0.125275	0.268

majority and the minority spin manifolds that controls the change in moment. When this quantity is positive, one expects the moment to increase. On the other hand, when this quantity is highly negative, an addition of H would lead to a decrease in the magnetic moment. To show this correlation, we list in Table 2, the HOMO and LUMO of all the clusters. Note that when δE is less than 0 eV, the spin magnetic moment does decrease upon addition of H_2. When δE is close to or more than 0 eV, the spin magnetic moment increases or varies little upon addition of H_2.

According to above analysis, it again identify the difference between the LUMO of the majority and the minority spin manifolds that controls the change in magnetic moment, the change rule in magnetic moment is different when H_2 is adsorbed on different transitional metal clusters. The model may be predict the change in magnetic moment when small molecular is adsorbed on the transitional metal clusters.

Conclusions

We have presented a systematic study on the interaction of the hydrogen atoms with the small Ru_n clusters in the size range of two to eight Ru atoms. The lowest energy structures of Ru_nH_2 clusters can be obtained by substituting H_2 in the lowest energy and some meta-stable isomers of Ru_n clusters. For $n > 2$, three different adsorption

patterns are found for the Ru_nH_2 complexes: One H atom binds to the Ru top site, and another H binds to the bridge site for $n = 3, 5, 6, 8$; bridge site adsorption for $n = 4$; hollow site and top site adsorption for $n = 7$. The adsorption energies display oscillation and reach the peak at $n = 2, 4, 7$, implying their high chemical reactivity. The small electron transferred number between H atoms and Ru_n clusters indicates the interaction between H atoms and Ru_n clusters is small. It is interesting to note that in all cases, the absorbed species does not lead to a rearrangement of the basic cluster. When H_2 is absorbed on the Ru_n clusters, the chemical activity of corresponding clusters is dramatically increased. The present studies show that the H absorption can lead to an oscillatory behavior of the magnetic moments. This behavior is rooted in the electronic structure of the preceding cluster and the changes in the magnetic moment are indicative of the relative ordering of the majority and minority LUMO's. The second order difference indicates 5 is magic number in Ru_nH_2 and Ru_n clusters.

Acknowledgments This project supported by foundation start up for high level talents of shihezi university, china (Grant No: RCZX200747).

Open Access This article is distributed under the terms of the Creative Commons Attribution Noncommercial License which permits any noncommercial use, distribution, and reproduction in any medium, provided the original author(s) and source are credited.

References

1. J. T. Stuckless, C. E. Wartnaby, N. Al-Sarraf, St. J. B. Dixon-Warren, M. Kovar, and D. A. King (1997). *J. Chem. Phys.* **106**, 2012.
2. R. Schaub, P. Thostrup, N. Lopez, E. Laegsgaard, I. Stensgaard, J. K. Nørskov, and F. Besenbacher (2001). *Phys. Rev. Lett.* **87**, 266104.
3. K. C. Prince, G. Paolucci, and A. M. Bradshaw (1986). *Surf. Sci.* **175**, 101.
4. D. A. Outka, J. Stöhr, W. Jark, P. Stevens, J. Solomon, and R. J. Madix (1987). *Phys. Rev. B* **35**, 4119.
5. B. E. Salisbury, W. T. Wallace, and R. L. Whetten (2000). *Chem. Phys.* **262**, 131.
6. L. Holmgren and A. Rosén (1999). *J. Chem. Phys.* **110**, 2629.
7. M. Balooch, M. J. Cardillo, D. R. Miller, and R. E. Stickney (1978). *Surf. Sci.* **46**, 358.
8. B. E. Hayden and C. L. A. Lamont (1989). *Phys. Rev. Lett.* **63**, 1823.
9. A. C. Luntz, J. K. Brown, and M. D. Williams (1990). *J. Chem. Phys.* **93**, 5240.
10. C. T. Rettner, D. J. Auerbach, and H. A. Michelsen (1992). *Phys. Rev. Lett.* **68**, 1164.
11. R. Linke, U. Schneider, H. Busse, C. Becker, U. Schroeder, G. R. Castro, and K. Wandelt (1994). *Surf. Sci.* **307**, 407.
12. U. Schneider, H. Busse, R. Linke, G. R. Castro, and K. Wandelt (1994). *J. Vac. Sci. Technol. A* **12**, 2069.
13. P. M. Holmblad, J. H. Larsen, and I. Chorkendorff (1996). *J. Chem. Phys.* **104**, 7289.
14. A. T. Pasteur, St. J. Dixon-Warren, Q. Ge, and D. A. King (1997). *J. Chem. Phys.* **106**, 8896.
15. B. Fruberger, J. Eng Jr., and J. G. Chen (1997). *Catal. Lett.* **45**, 85.
16. A. Berces, P. A. Hackett, L. Lian, S. A. Mitchell, and D. M. Rayner (1998). *J. Chem. Phys.* **108**, 5476.
17. P. Samson, A. Nesbitt, B. E. Koel, and A. Hodgson (1998). *J. Chem. Phys.* **109**, 3255.
18. K. Moritani, M. Okada, M. Nakamura, T. Kasai, and Y. Murata (2001). *J. Chem. Phys.* **115**, 9947.
19. C. EibI and A. Winkler (2002). *J. Chem. Phys.* **117**, 834.
20. M. F. Somers, D. A. McCormack, G. J. Kroes, R. A. Olsen, E. J. Baerends, and R. C. Mowrey (2002). *J. Chem. Phys.* **117**, 6673.

21. P. Ravindran, P. Vajeeston, R. Vidya, A. Kjekshus, and H. Fjellvag (2002). *Phys. Rev. Lett.* **89**, 106403.
22. A. Pramann (2001). *J. Chem. Phys.* **115**, 5404.
23. E. Poulain, J. I. Benítez, S. Castillo, V. Bertin, and A. Cruz (2004). *J. Mol. Struct. (Theochem.)* **709**, 67.
24. H. Strφmsnes, S. Jusuf, B. Schimmelpfenning, U. Wahlgren, and O. Gropen (2001). *J. Mole. Struct.* **137**, 567.
25. R. L. Whetten, D. M. Cox, D. J. Trevor, and A. Kaldor (1985). *Phys. Rev. Lett.* **54**, 1494.
26. M. B. Knickelbein, G. M. Koretsky, K. A. Jackson, M. R. Pederson, and Z. Hajnal (1998). *J. Chem. Phys.* **109**, 10692.
27. M. B. Knickelbein (1999). *Ann. Rev. Phys. Chem.* **50**, 79.
28. S. P. Liu, C. Hao, S. M. Li, and Z. X. Wang (2009). *Appl. Sur. Sci.* **225**, 4232.
29. C. Crisafulli, S. Scirè, S. Minicò, and L. Solarino (2002). *Appl Catal A: General* **225**, 1.
30. R. Berthoud, P. Délichère, D. Gajan, W. Lukens, K. Pelzer, J. M. Basset, J. P. Candy, and C. Copéret (2008). *J. Catal.* **260**, 387.
31. W. Q. Zheng, J. Zhang, H. Y. Xu, and W. Z. Li (2007). *Catal. Lett.* **119**, 311.
32. X. Y. Tu, D. W. Wang, and X. M. Chen (2004). *Precious Metals* **25**, 15.
33. G. Suss-Fink (2000). *J. Organomet. Chem.* **609**, 196.
34. R. D. Adams, B. Captain, C. Beddie, and M. B. Hall (2007). *J. Am. Chem. Soc.* **129**, 986.
35. R. D. Adams, B. Captain, and L. Zhu (2007). *J. Am. Chem. Soc.* **129**, 2454.
36. R. D. Adams, B. Captain, M. D. Smith, C. Beddie, and M. B. Hall (2007). *J. Am. Chem. Soc.* **129**, 5981.
37. R. D. Adams, E. M. Boswell, M. B. Hall, and X. Yang (2008). *Organometallics* **27**, 4938.
38. I. Rosal, L. Truflandier, R. Poteau, and I. C. Gerber (2011). *J. Phys. Chem. C* **115**, 2169.
39. T. Gutmann, B. Walaszek, Y. P. Xu, M. Wächtler, I. del Rosal, A. GrOnberg, R. Poteau, R. Axet, G. Lavigne, B. Chaudret, H. H. Limbach, and G. Buntkowsky (2010). *J. Am. Chem. Soc.* **132**, 11759.
40. B. Delley (1990). *J. Chem. Phys.* **92**, 508.
41. R. S. Mulliken (1955). *J. Chem. Phys.* **23**, 1841.
42. J. Andzelm, E. Radzio, and D. R. Salahub (1985). *J. Chem. Phys.* **83**, 4573.
43. H. Wang, Y. Liu, H. Haouari, R. Craig, J. R. Lombardi, and D. M. Lindsay (1997). *J. Chem. Phys.* **106**, 6534.
44. D. R. Lide (ed.) *CRC handbook of chemistry and physics, 79th* (CRC Press, New York, 1998), pp. 9–80.
45. X. Y. Tu, D. W. Wang, and X. M. Chen (2004). *Chin. J. Struct. Chem.* **23**, 940.
46. T. J. Dhilip Kumar, P. F. Weck, and N. Balakrishnan (2007). *J. Phys. Chem. C* **111**, 7494.
47. M. Fichtner, O. Fuhr, O. Kircher, and J. Rothe (2003). *Nanotechonlogy* **14**, 778.
48. R. Fournier and D. R. Salahub (1990). *Surf. Sci.* **238**, 330.
49. C. Ashman, S. N. Khanna, and M. R. Pederson (2003). *Chem. Phys. Lett.* **368**, 257.